Contact Metamorphism Around the Eocene Saraycık Granodiorite, Eastern Pontides, Turkey

GÜLTEKİN TOPUZ

İstanbul Teknik Üniversitesi, Avrasya Yerbilimleri Enstitüsü, TR–34469 Ayazağa, İstanbul, Turkey
(E-mail: topuzg@itu.edu.tr)

Abstract: The Eocene Saraycık granodiorite, eastern Pontides, Turkey, is a small post-tectonic intrusive body (~11 km^2), cross-cutting tectonically juxtaposed distinct metamorphic and non-metamorphic lithologies. A ~0.8 to 1-km-wide contact-metamorphic aureole has developed around the intrusion. Disequilibrium is prevalent in all lithologies, even in the inner zones of the contact aureole. Conditions of contact metamorphism are estimated by simple phase equilibria applied to microdomains in the metapelitic lithologies without obvious signs of disequilibrium: Shallow emplacement depths (0.21±0.05 GPa = ~5–8 km) are suggested by contact-metamorphic mineral assemblages (e.g., andalusite + corundum + K-feldspar), by Al-in-hornblende barometry on granodiorite and by partial melting within the stability field of andalusite near the intrusive contact. Peak temperatures during the contact metamorphism ranged from 430–520 °C at the outer domains of the aureole (~400 m from the intrusive contact) to ≥730 °C at the immediate contact of the intrusion. Textural evidence for partial melting in the stability fields of both andalusite and sillimanite are observed in metapelitic lithologies at distances ≤30 m from the intrusive contact. Basic lithologies contain mostly foliation-parallel, 2–50-mm-thick layers with skarn-like mineralogy, which probably formed via infiltration of chemically reactive fluids. Prevalence of disequilibrium is predominantly related to temporal variation in temperature and/or fluid composition attending the contact metamorphism, rather than to the presence of some relict minerals from a pre-contact-metamorphic stage.

Key Words: contact metamorphism, disequilibrium, andalusite + melt stability, *P-T* estimates, Saraycık granodiorite, eastern Pontides, Turkey

Eosen Yaşlı Saraycık Granodiyoritinin Çevresindeki Dokanak Başkalaşımı (Doğu Pontidler, Türkiye)

Özet: Eosen yaşlı Saraycık granodiyoriti, Bayburt, Doğu Pontidler, tektonizma sonrası yerleşmiş küçük bir sokulum kütlesi olup (yaklaşık 11 km^2), tektonik olarak yanyana getirilmiş farklı nitelik ve yaştaki metamorfik ve metamorfik olmayan kayaçları kesmektedir. Sokulum sonucunda çevreleyen kayaçlarda ~0.8–1 km genişliğinde bir dokanak başkalaşım halesi gelişmiştir. Bütün litolojilerde ince kesit ölçeğinde dengesizlik dokuları, başkalaşım halesinin iç zonlarında bile, yaygınca gözlenmektedir. Dokanak başkalaşımının koşulları, metapelitlerde bariz bir dengesizlik belirtisi göstermeyen mikro-alanlara uygulanan faz dengeleri ile tahmin edildi: Dokanak başkalaşımı sonucunda oluşan mineral toplulukları (sözgelimi, andaluzit + korund + K-feldspat), granodiyoritin içerdiği hornblendlerin Al içeriklerine dayalı olarak yapılan basınç tahmini ve andaluzit durağanlık alanında bölümsel ergime sığ yerleşim derinliklerine işaret etmektedir (0.21±0.05 GPa = ~5–8 km). Dokanak başkalaşımı sırasında, doruk sıcaklıkları dokanaktan 400 m uzakta 430–520 °C'den dokanağın bitişiğinde ≥730 °C'ye kadar değişmektedir. Sokulum dokanağından ≤30 m uzaklıklarda pelitik litolojiler, gerek andaluzit gerekse sillimanit durağanlık alanlarında bölümsel ergimeye uğramış olduklarının izlerini taşımaktadır. Bazik litolojiler genelde yapraklanmaya paralel uzanan, 2–50 mm kalınlığında ve skarnlara benzer mineraloji sunan seviyeler içermektedir. Bu seviyeler olasılıkla akışkanların bazik litolojilerle etkileşimi sonucunda oluşmuştur. Dengesizlik dokuların yaygınlığı baskın olarak dokanak başkalaşımı öncesi aşamadan kalıntı varlığından ziyade, dokanak başkalaşımı sırasında sıcaklık ve/veya akışkan kimyasının zamansal değişimiyle bağlantılıdır.

Anahtar Sözcükler: dokanak başkalaşımı, dengesizlik, *P-T* tahmini, andaluzit + ergiyik durağanlığı, Saraycık granodiyoriti, Doğu Pontidler, Türkiye

Introduction

Contact metamorphism results from thermal perturbation at a given depth caused by the emplacement of igneous intrusions into cooler rocks, and is characterized by shorter time scales for heating and cooling relative to regional metamorphism (Kerrick 1991). Disequilibrium in contact-metamorphic mineral assemblages is widespread due to kinetic factors and/or temporal variation in intensive parameters, even in the inner zones of aureoles where high temperatures are attained and reaction rates are expected to be high (e.g., see Clechenko & Valley 2003; Wheeler *et al.* 2004 and references therein). However, *P-T* estimates across a contact aureole are mostly based on equilibrium assemblages (e.g., Pattison 1989; Droop *et al.* 2003). Hence, determination of equilibrium mineral assemblages is an important task, and can be made by means of careful microtextural investigations.

The geological structure of the eastern Pontides, NE Turkey, is the result of long-lived subduction, accretion and collision events related to the closure of the Tethyan ocean (Okay & Şahintürk 1997 and references therein). As a consequence, granitoids – ranging in age from Late Carboniferous to Eocene – are widely exposed throughout the eastern Pontides (e.g., Boztuğ *et al.* 2004 and references therein; Karslı *et al.* 2004; Aslan 2005; Yılmaz-Şahin 2005). These granitoids are generally shallow-level intrusions. Their contact aureoles have, however, received scant attention (e.g., Taner 1977; Sadıklar 1993).

The Saraycık granodiorite in the Bayburt region of the eastern Pontides is a relatively simple intrusive body emplaced into tectonically juxtaposed lithologies, thereby giving an unusual opportunity to study the responses of distinct lithologies to a common thermal perturbation. This paper presents a detailed description of the spatial distribution and textural relationships of the contact-metamorphic mineral assemblages in the various lithologies around the Saraycık granodiorite, and estimates *P-T* conditions across the contact aureole.

Geological Setting and Saraycık Contact Aureole

The Saraycık area in the Bayburt region of the eastern Pontides forms part of a Late Palaeocene to Early Eocene north-vergent fold-and-thrust belt (Figure 1; Okay & Şahintürk 1997; Okay *et al.* 1997). The Saraycık granodiorite is a small intrusion with an outcrop area of ~11 km^2, and postdates the development of this thrust-and-fold belt, cross-cutting the tectonic contact between two thrust sheets: the Hamurkesen and Aşutka (Figures 1 & 2; Okay 1996; Topuz *et al.* 2005). The intrusion forms a rather flat topography in contrast to the older country rocks, and is made up mainly of fine- to medium-grained hornblende-biotite and hornblende-free biotite granodiorites, cross-cut by comagmatic ≤ 10-m-thick dacitic dikes and ≤ 25-cm-thick aplite and late quartz veins. Its emplacement is dated as ~52 Ma (Ypressian, Eocene) by two stepwise $^{40}Ar/^{39}Ar$ biotite ages, which also provide a minimum age constraint for the development of the fold-and-thrust belt (Topuz *et al.* 2005). The granodiorite displays close compositional similarities to high-silica adakites from supra-subduction settings, and is thought to have derived from the partial melts of mafic lower crust in a post-collisional environment on the basis of geochemical and regional geological constraints (Topuz *et al.* 2005).

The granodiorite intrusion resulted in the development of a ~0.8- to 1-km-wide contact metamorphic aureole visible in (a) Permian low-grade and Carboniferous high-grade metamorphic rocks of the Pulur complex in the Aşutka sheet, and (b) Late Carbonifeous non-metamorphic sedimentary rocks and discordantly overlying Liassic basal conglomerate and volcanoclastic rocks of the Hamurkesen thrust sheet (Figures 1 & 2). Permian low-grade and Carboniferous high-grade metamorphic units are separated by a pre-Liassic thrust (Okay 1996; Topuz *et al.* 2004a, b). The intrusive contacts are sharp, and there is no evidence for downward and/or upward drag of country rocks adjacent to the contact. Within the contact-metamorphic aureole, bedding and regional-metamorphic foliations are, albeit attenuated, mostly preserved right up to the igneous contact (Figure 3). The use of the term "hornfels" is, therefore, not justified for referring to the rock types inside the contact aureole.

Analytical Techniques

Mineral analyses were carried out with a five spectrometer CAMECA-SX51 electron microprobe equipped with five wavelength-dispersive spectrometers and an additional Si-Li detector (LINK-ISIS, Oxford Instruments) at the Mineralogical Institute of Heidelberg
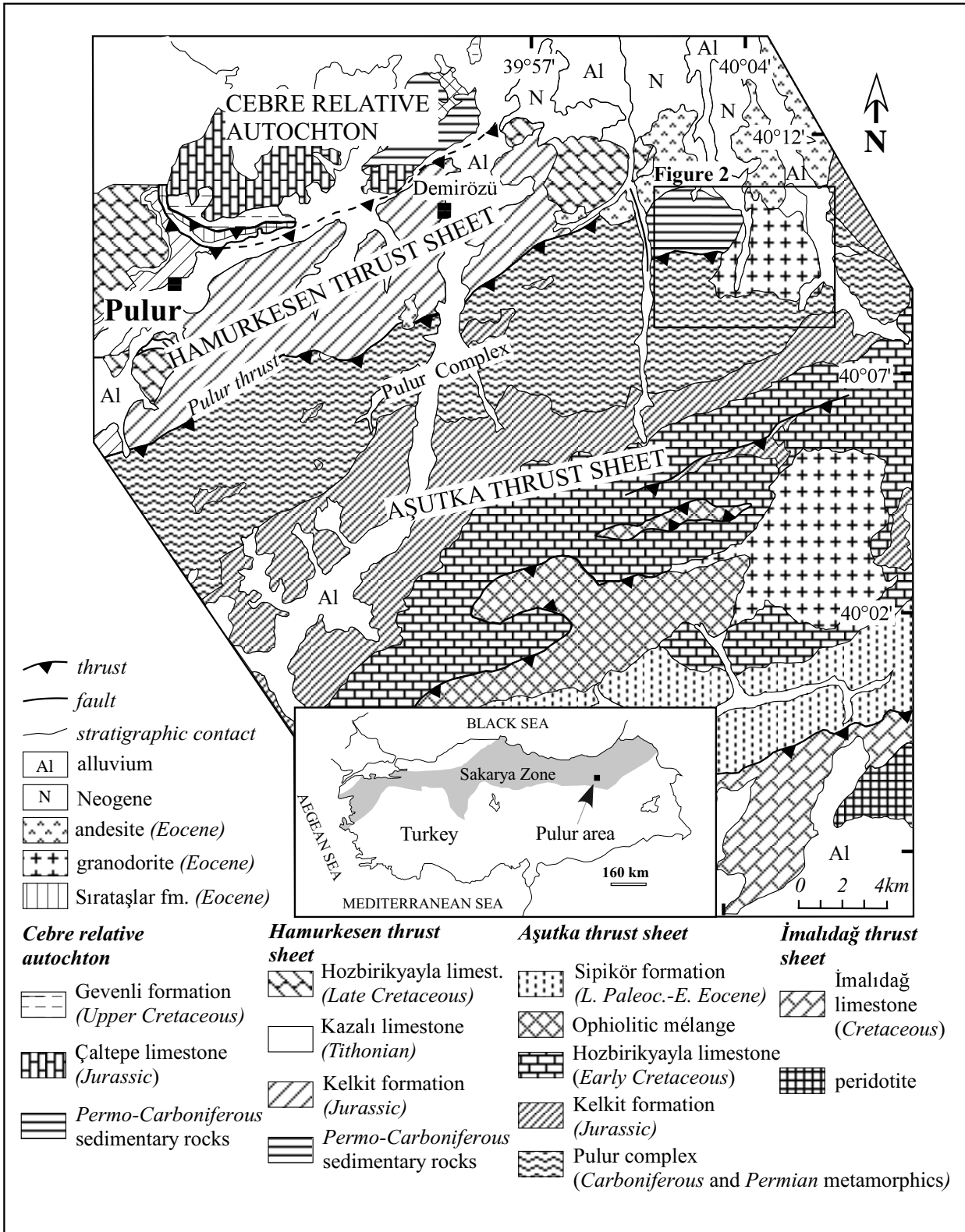
Figure 1. Generalized geological map of the Pulur area (modified after Okay *et al.* 1997). Inset shows the location of the Pulur area in Turkey.
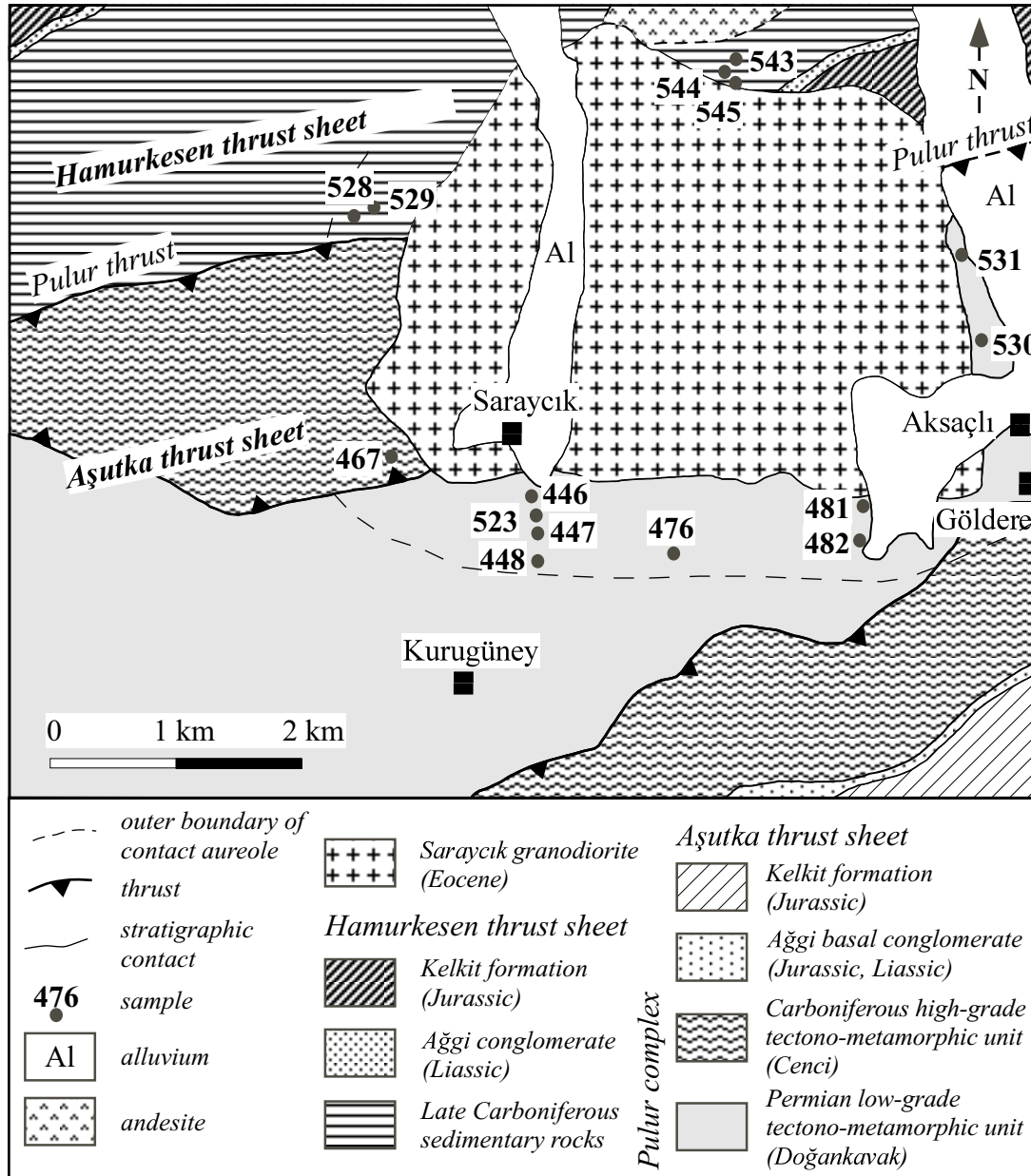
Figure 2. Geological map of the Saraycık granodiorite and its contact-metamorphic aureole with sample locations (modified after Topuz *et al.* 2005).

University (Germany). Natural and synthetic oxide and silicate standards were used for calibration before each measurement session. Standard operating conditions were a 15 kV accelerating voltage, 20 nA beam current and 10 s counting times for all the elements except for those in Fe-Ti oxides and feldspars. The counting times during the Fe-Ti oxide analyses were 20 s for Mg, Ca and

Al, and 30 s for Ti. A beam size of 1 μm was used in these analyses except for feldspars. Feldspar analyses were conducted on a beam size of ~ 10μm to minimize the alkali loss due to volatilization. Raw data were corrected for matrix effects with the help of the PAP algorithm (Pouchou & Pichoir 1984, 1985) implemented by CAMECA.
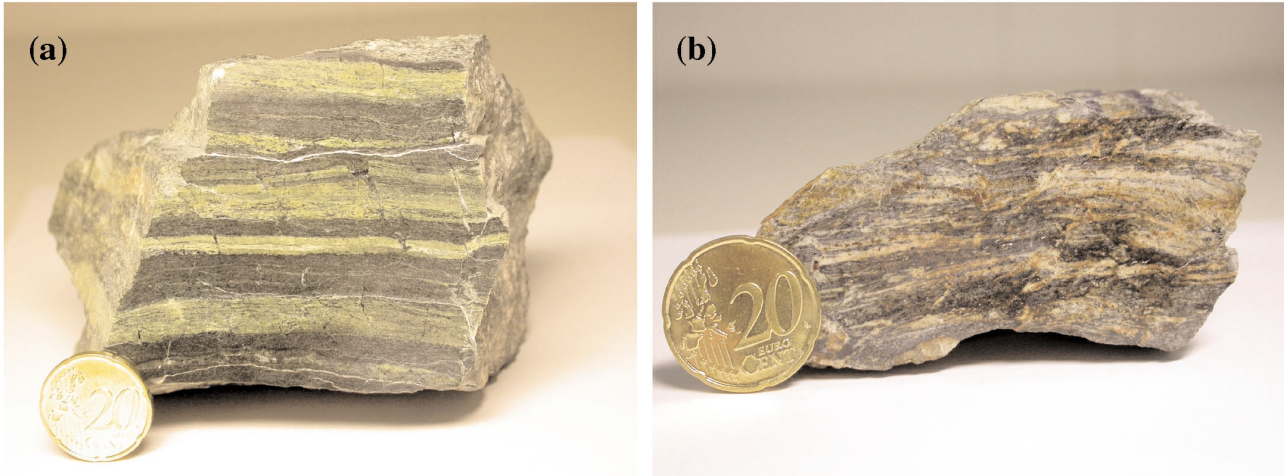
Figure 3. Photographs of hand specimens with well-preserved relict foliation: **(a)** a metabasite with foliation-parallel yellow layers consisting of epidote + quartz + calcite; the dark green domain is made up of hornblende/actionolite + epidote + plagioclase (sample 447); **(b)** foliation-parallel leucosomes in a former phyllite (sample 531). Leucosomes are discontinuous. The coin is 2.2 cm across.

Petrography and Mineral Compositions

Contact-metamorphic effects in the Liassic volcanoclastic rocks (Kelkit Formation) were not investigated. Mineralogical compositions and the estimated modes of the studied samples are given in Table 1. The approximate outer boundary of the contact aureole is based on the first appearance of plagioclase with An≥15 and/or biotite in low-grade and nonmetamorphic rocks (Figure 2). Due to the limited number of samples investigated, the outer limit of the contact aureole in the high-grade metamorphic rocks remains unconstrained. The spatial distributions of the rock types around the intrusion do not allow the drawing of any isograds.

Permian Low-grade Tectono-metamorphic (Doğankavak) Unit

The Doğankavak unit, which abuts the southern and western margin of the intrusion, underwent Permian greenschist- to albite-epidote-amphibolite-facies metamorphism (400–470 °C; 0.6–1.1 GPa and 260 Ma BP, Topuz *et al.* 2004a), and is represented by metabasites and phyllites within the contact aureole (Figure 2). Outside the contact aureole, the metabasites contain the mineral assemblage "Hbl/Act + Ep + Chl + Ab (An<04) + Qtz ± Phe + Ttn ± Mag", and phyllites "Phe + Chl + Ab (An<04) + Qtz + Rt ± Tur ± Cal" (all the mineral

abbreviations are after Kretz 1983). Grain sizes outside the contact aureole are in the range of ~100–200 μm in the metabasites, and ~25–100 μm in the phyllites.

At distances ≥ 500 m from the intrusive contact, the *metabasites* (samples 448 and 476) differ from those outside the contact aureole by the presence of oligoclase with An≥15 (Table 1). Transition from albite to oligoclase with An≥15 is not abrupt: oligoclase with An≥15 unevenly grows on some albite grains. Approaching the intrusive contact (samples 446a, 446b, 447, 481C and 523), primary chlorite disappears and either epidote disappears or its amount decreases, giving rise to the mineral assemblage Hbl ± Act + Pl ± Ep + Qtz ± Bt + Mag + Ilm + Rt + Ttn. Texturally and compositionally, three generations of amphibole can be distinguished (Figure 4a, b): hornblende-1 (Hbl_1) represents the oldest, and contains patchy domains of actinolite (Act). Both are unevenly overgrown by Fe- and Al-richer hornblendes (Hbl_2). Amphibole compositions, consequently, range from actinolite through magnesiohornblende to pargasite (Figure 5a; Table 2). Outside the contact aureole, amphiboles are hornblende – with/without actinolitic core – which is compositionally similar to Hbl_1 and Act within the contact aureole (cf. Topuz *et al.* 2004a). In contrast to the regional metamorphic actinolites, contact metamorphic ones occur as patchy domains within Hbl_1. Plagioclases display patchy domains of distinct compositions, ranging in composition from An_{09} to An_{98},

Table 1. Mineral assemblages of studied samples from the Saraycik contact aureole.

Sample	Hbl/Act	Ep	Chl	Pl	Qtz	Ttn	Mag	Ilm	Cpx	Grt	Cal	Wol	Ms	Bt	Mrg	And	Sil	Crn	Spl	Kfs	Tur	Apa	Zrn	Mnz
Low-grade tectonometamorphic unit (Doğankavak)																								
446A	++	o	–	++	o	o	o	–	–	–	–	–	–	–	–	–	–	–	–	–	–	–	–	–
446A-L	o	++	–	+	–	–	o	–	++	–	–	–	–	–	–	–	–	–	–	–	–	–	–	–
446B	++	–	–	++	–	o	o	–	–	–	–	–	–	–	–	–	–	–	–	–	–	–	–	–
447	++	o	–	++	–	o	o	–	–	–	–	–	–	–	–	–	–	–	–	–	–	–	–	–
447-L	–	++	–	+	o	o	o	o	++	++	+	o	–	–	–	–	–	–	–	–	–	–	–	–
448	++	++	+	++	o	+	o	o	–	–	–	–	–	–	–	–	–	–	–	–	–	–	–	–
448-L	–	++	+	–	+	o	–	–	–	–	+	–	–	–	–	–	–	–	–	–	–	–	–	–
476	++	++	+	++	–	+	–	o	–	–	–	–	–	–	–	–	–	–	–	–	–	o	–	–
481C	++	++	–	++	+	o	o	–	–	–	+	–	–	–	–	–	–	–	–	–	–	–	–	–
481C-L	–	–	–	++	+	+	+	–	++	++	–	–	–	–	–	–	–	–	–	–	–	–	–	–
523	++	+	–	+	o	+	–	–	–	–	–	–	–	–	–	–	–	–	–	–	–	–	–	–
523-L	–	+	–	++	+	o	o	–	++	++	o	–	–	–	–	–	–	–	–	–	–	–	–	–
487	++	+	–	++	–	+	o	–	–	–	–	–	–	–	–	–	–	–	–	–	–	–	–	–
481-Mm	–	–	–	++	o	–	–	–	–	–	–	–	+,s	++	+,s	+	–	o	–	o	o	o	o	o
481-Lm	–	–	–	+	++	–	–	–	–	–	–	–	–	–	–	–	–	–	–	++	–	–	–	–
482	–	–	–	++	++	–	–	o	–	–	–	–	++	+	–	+	–	–	–	–	o	o	–	o
531-Mm	–	–	–	++	o	–	–	–	–	–	–	–	+,s	++	+,s	+	–	o	–	o	o	o	o	o
531-Lm	–	–	–	+	++	–	–	–	–	–	–	–	–	–	–	–	–	–	–	++	–	–	–	–
High-grade tectonometamorphic unit (Cenci)																								
467	++	–	o,s	++	–	–	–	o	–	–	–	–	–	–	–	–	–	–	–	–	–	o	–	–
Late Carboniferous sedimentary rocks																								
528	–	–	–	–	++	–	–	o	–	–	–	–	++	+	–	–	–	–	–	–	o	o	o	o
544B	–	–	o,s	–	+	–	–	o	–	–	–	–	+,s	++	–	–	o	o	o	o	–	o	o	o
545	–	–	–	–	+	–	–	o	–	–	–	–	+,s	++	–	–	o	o	o	+	–	o	o	o

++ major constituent, + minor constituent, o accessory phase, – not observed , s secondary, L yellow to brown layers, Lm leucosome, Mm: mesosome
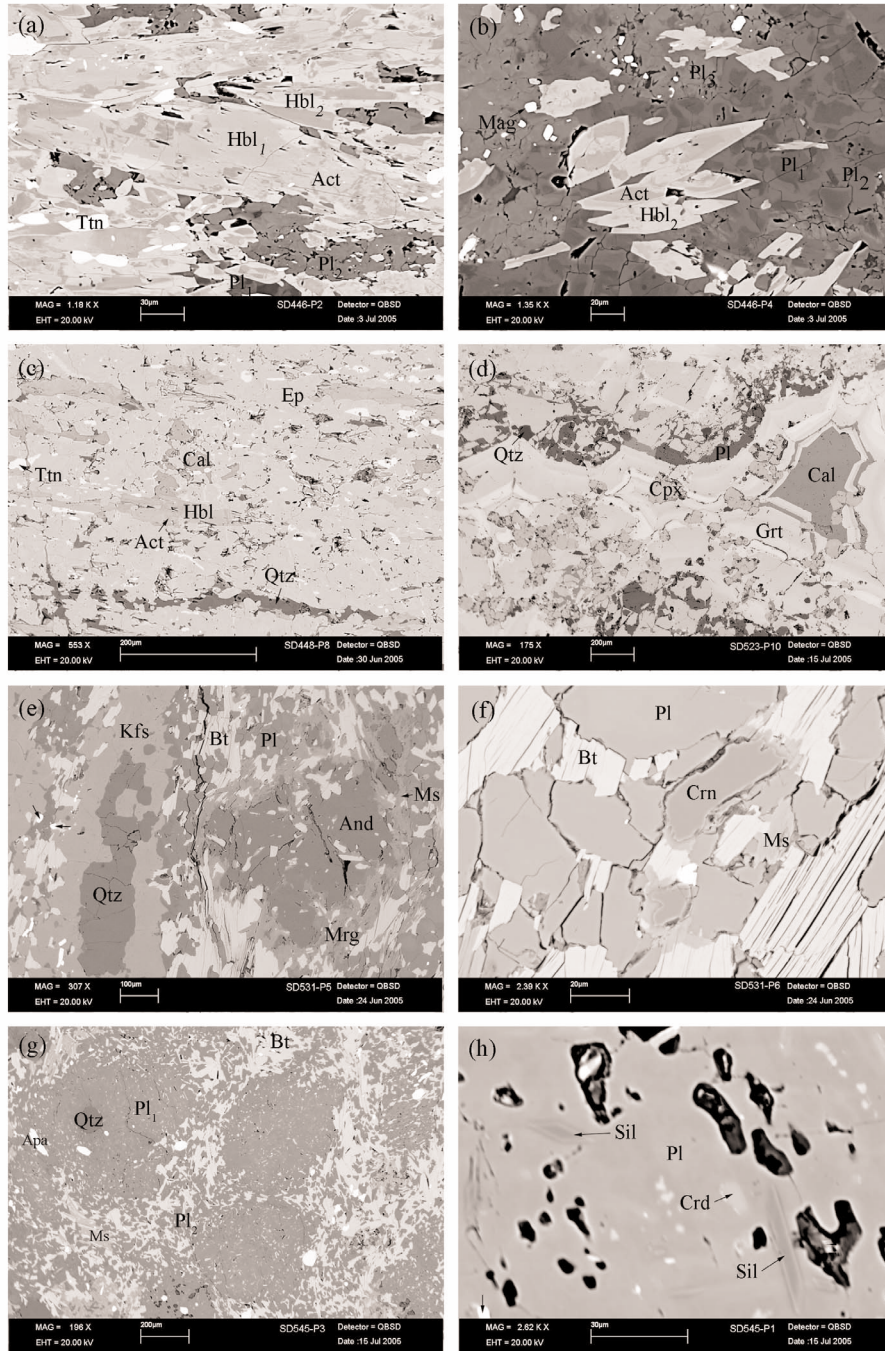
Figure 4. Back-scattered electron images showing microtextural features of the contact-metamorphic mineral assemblages: **(a)** Compositionally different types of amphiboles (Hbl_1, Hbl_2 and Act). Hbl_1 represents the cores of amphiboles, which is irregularly replaced by actinolite (Act). Both Act and Hbl_1 are, in turn, overgrown by Hbl_3 (sample 446); **(b)** amphiboles with actinolitic (Act) cores and hornblendic rims (Hbl_2) in a plagioclase matrix ranging in composition from albitic (Pl_1) through intermediate (Pl_2) to an anorthite-rich one (Pl_3, sample 446); **(c)** epidote (Ep), Hbl/Act, titanite (Ttn), calcite (Cal) and quartz (Qtz) from a yellow layer in the metabasite (sample 448); **(d)** a microdomain within the brown layers consisting of garnet (Grt), clinopyroxene (Cpx), Cal and Qtz. Garnet displays oscillatory zoning: bright zones represent andradite-rich, and darker zones grossular-rich compositions (sample 523); **(e)** an andalusite (And) porphyroblast in melanosome with inclusions of biotite (Bt). Andalusite is irregularly replaced marginally by margarite (Mrg) and muscovite (Ms). Coarser Qtz and K-feldspar (Kfs) make up the leucosome (sample 531); **(f)** tiny grains of corundum (Crn) in the melanosome, marginally replaced by Ms (sample 531); **(g)** inclusion-rich Pl porphyroblasts in a matrix consisting of fine-grained Pl, Bt and secondary Ms (sample 545); **(h)** Sillimanite (Sil), cordierite (Crd) and spinel (Spl) inclusions in the large Pl porphyroblast (sample 545).
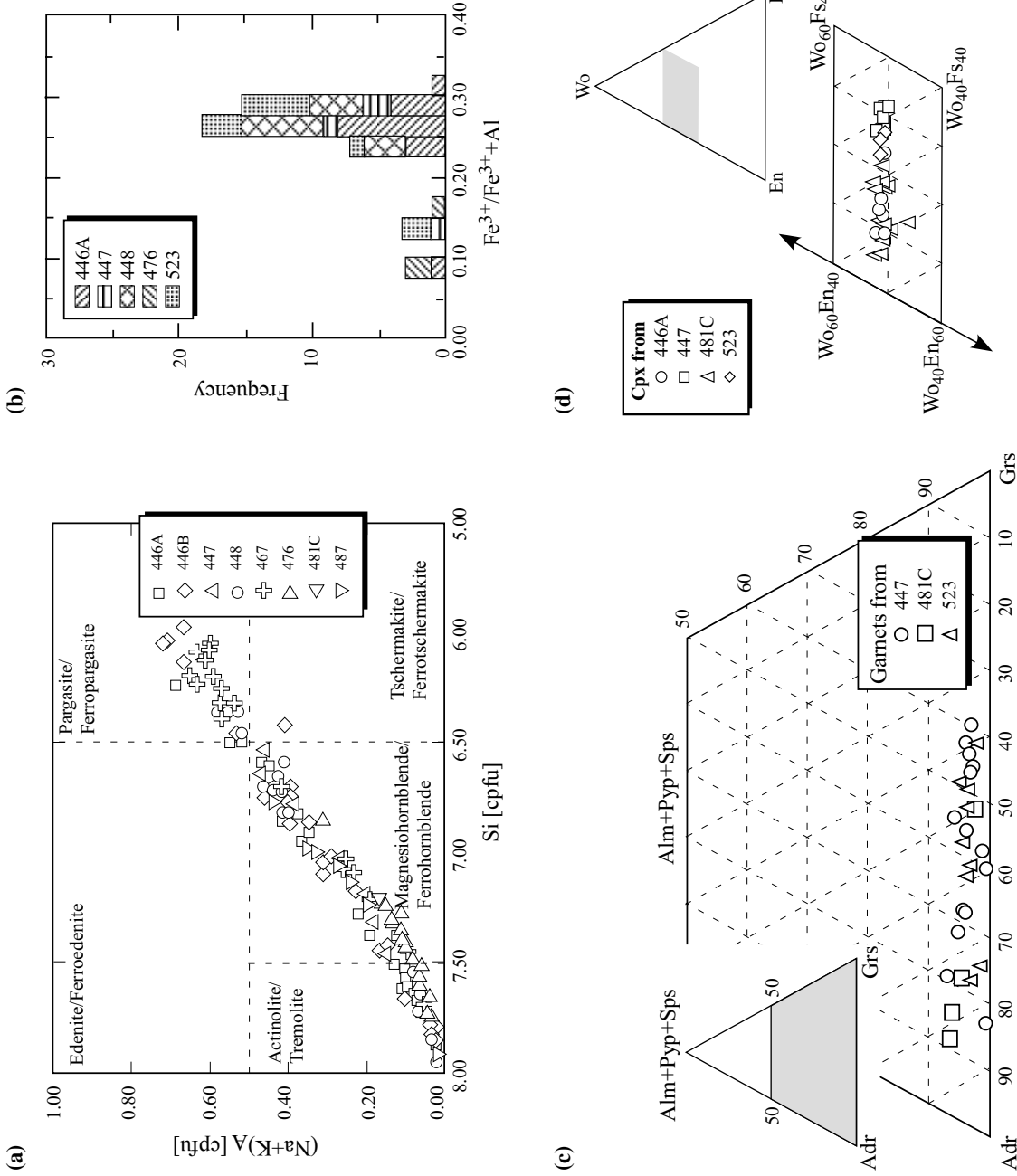
Figure 5. Compositional variation of minerals from the metabasites: (a) amphiboles in terms of Si and (Na+K)$_A$ (modified after Leake *et al.* 1997); (b) epidotes in terms of Fe^{3+}/(Al+Fe^{3+}); (c) garnets in the ternary diagram (Pyp+Alm+Sps)-Adr-Grs; (d) clinopyroxenes in the ternary diagram Wo-En-Fs.

Table 2. Selected representative electron-microprobe analyses of amphiboles and plagioclases from metabasic lithologies, Saraycik contact aureole.

Sample	446A	446A	446A	446B	447	447	448	448	467	467	476	476	481c	481c	446A	446A	446B	446B	447	447	448	448	467	467
Mineral	Am	Am	Am	Am	Am	Am	Am	Am	Am	Am	Am	Am	Am	Am	Pl	Pl	Pl	Pl	Pl	Pl	Pl	Pl	Pl	Pl
Analyse	2	3	14	45	62	90	11	65	24	23	21	68	26	75	3	14	3	45	62	90	11	65	39	40
SiO_2	47.76	55.35	43.68	40.82	43.33	51.01	54.20	42.96	48.63	42.47	44.99	52.33	40.88	53.29	44.57	67.09	57.93	68.03	59.93	69.41	48.85	42.42	44.03	43.62
TiO_2	0.31	0.00	0.57	0.74	0.51	0.32	0.08	0.57	0.14	0.55	0.24	0.14	1.57	0.17	0.00	0.00	0.02	0.00	0.02	0.02	0.00	0.03	0.00	0.00
Al_2O_3	8.36	1.44	10.10	13.90	10.61	4.09	2.06	13.01	8.82	14.43	9.06	2.25	12.32	2.66	36.24	21.43	26.79	20.50	24.54	19.40	31.90	35.66	36.43	36.55
Cr_2O_3	0.03	0.00	0.08	0.18	0.00	0.04	0.00	0.24	0.02	0.09	0.02	0.00	0.32	0.08	0.00	0.00	0.01	0.00	0.03	0.00	0.00	0.00	0.00	0.00
FeO	13.40	9.92	16.51	16.60	18.60	13.17	12.78	14.02	10.57	12.44	19.47	18.20	13.94	9.81	0.31	0.38	0.27	0.26	0.48	0.20	0.08	0.39	0.27	0.09
MnO	0.46	0.41	0.46	0.30	0.37	0.37	0.43	0.31	0.25	0.26	0.28	0.37	0.35	0.29	0.00	0.00	0.00	0.00	0.07	0.00	0.00	0.04	0.00	0.00
MgO	13.02	17.51	10.81	9.92	9.70	14.48	15.65	11.94	15.24	12.22	8.80	11.81	11.86	17.49	0.00	0.00	0.01	0.00	0.24	0.04	0.01	0.02	0.00	0.00
CaO	11.72	12.24	11.98	11.79	11.80	12.58	12.28	10.84	11.94	11.56	11.81	12.26	12.23	12.78	19.43	1.88	8.75	0.73	7.29	0.15	15.60	19.45	19.65	19.78
Na_2O	1.35	0.30	1.43	2.34	1.51	0.55	0.29	2.23	1.29	2.22	0.86	0.16	1.92	0.33	0.74	10.84	6.76	11.44	7.41	11.77	2.76	0.45	0.63	0.47
K_2O	0.07	0.03	0.45	0.20	0.38	0.05	0.06	0.33	0.06	0.15	0.49	0.07	1.01	0.14	0.02	0.07	0.07	0.04	0.05	0.05	0.04	0.00	0.02	0.02
Total	96.46	97.20	96.07	96.79	96.81	96.66	97.82	96.43	96.96	96.40	96.02	97.59	96.39	97.04	101.31	101.69	100.59	101.00	100.05	101.03	99.24	98.46	101.03	100.53

Cations on the basis of 23 oxygens (Am*) and 8 oxygens (Pl)

Si	7.021	7.879	6.589	6.134	6.531	7.458	7.775	6.360	6.994	6.261	6.858	7.732	6.153	7.613	2.036	2.899	2.581	2.949	2.673	3.000	2.251	1.999	2.019	2.010
Ti	0.034	0.000	0.065	0.084	0.058	0.035	0.008	0.063	0.015	0.061	0.027	0.016	0.178	0.018	0.000	0.000	0.001	0.000	0.001	0.001	0.000	0.001	0.000	0.000
Al	1.449	0.242	1.795	2.462	1.883	0.705	0.348	2.270	1.495	2.507	1.628	0.391	2.184	0.448	1.951	1.092	1.407	1.048	1.290	0.989	1.732	1.981	1.969	1.985
Cr	0.003	0.000	0.009	0.031	0.000	0.004	0.000	0.028	0.003	0.015	0.002	0.000	0.038	0.008	0.000	0.000	0.000	0.000	0.001	0.000	0.000	0.000	0.000	0.000
Fe^{3+}	0.223	0.047	0.454	0.470	0.526	0.172	0.094	0.454	0.286	0.371	0.327	0.099	0.392	0.212	0.012	0.014	0.010	0.009	0.018	0.007	0.003	0.015	0.010	0.003
Fe^{2+}	1.424	1.134	1.629	1.617	1.818	1.438	1.439	1.282	0.985	1.163	2.155	2.149	1.363	0.960	0.000	0.000	0.000	0.000	0.000	0.000	0.000	0.000	0.000	0.000
Mn	0.057	0.049	0.058	0.038	0.047	0.047	0.053	0.038	0.030	0.033	0.036	0.047	0.045	0.035	0.000	0.000	0.000	0.000	0.002	0.000	0.000	0.002	0.000	0.000
Mg	2.853	3.715	2.432	2.222	2.180	3.156	3.348	2.636	3.267	2.686	2.001	2.601	2.660	3.726	0.000	0.000	0.000	0.000	0.016	0.003	0.002	0.002	0.000	0.000
Ca	1.845	1.867	1.936	1.898	1.906	1.971	1.887	1.719	1.840	1.826	1.928	1.941	1.972	1.957	0.951	0.087	0.418	0.034	0.348	0.007	0.770	0.982	0.965	0.976
Na	0.283	0.082	0.416	0.682	0.440	0.157	0.080	0.640	0.359	0.635	0.255	0.046	0.561	0.092	0.065	0.908	0.583	0.961	0.641	0.986	0.247	0.041	0.056	0.042
K	0.013	0.005	0.087	0.038	0.073	0.009	0.010	0.061	0.010	0.028	0.095	0.013	0.193	0.025	0.001	0.004	0.004	0.002	0.003	0.002	0.002	0.000	0.001	0.001
Mg#	0.67	0.77	0.60	0.58	0.55	0.69	0.70	0.67	0.77	0.70	0.48	0.55	0.66	0.80	-	-	-	-	-	-	-	-	-	-
X_{Na}	-	-	-	-	-	-	-	-	-	-	-	-	-	-	0.06	0.91	0.58	0.96	0.65	0.99	0.24	0.04	0.06	0.04
X_{Ca}	-	-	-	-	-	-	-	-	-	-	-	-	-	-	0.93	0.09	0.42	0.03	0.35	0.01	0.76	0.96	0.94	0.96
X_{K}	-	-	-	-	-	-	-	-	-	-	-	-	-	-	0.00	0.00	0.00	0.00	0.00	0.00	0.00	0.00	0.00	0.00

* Calculation method of Schumacher (1997), Mg# $Mg/(Mg+Fe^{2+})$, X_{Na} $Na/(Na+Ca+K)$, X_{Ca} $Ca/(Na+Ca+K)$, X_{K} $K/(Na+Ca+K)$

even in a single thin section (Figure 4a, b; Table 2): Apart from the albitic plagioclases (Pl_1), there are at least two distinct compositional plagioclase types, one intermediate (Pl_2) and one anorthite-rich (Pl_3), none of which share straight grain boundaries with each other. As the plagioclases outside the aureole have albitic compositions (An≤04), these albitic plagioclases can be regarded as relict from regional metamorphism, and Pl_2 and Pl_3 must have formed during contact metamorphism. Epidotes are characterized by $Fe^{3+}/(Fe^{3+}+Al)$ values of 0.07–0.31, and most compositions cluster around 0.22–0.32 (Figure 5b; Table 3). Epidotes outside the contact aureole show comparatively wide variation in $Fe^{3+}/(Fe^{3+}+Al)$ values (0.14–0.35). Titanite displays Al_2O_3 and Fe_2O_3 contents of 0.60–2.30 and 0.50–1.60 wt %, respectively, and ilmenites have appreciable MnO contents (2.12–3.51 wt %; Table 3). Rutile is rimmed by titanite in many cases. There is generally no perceptible change in the grain size of the metabasites towards the intrusive contact. One conspicuous feature of the metabasites is the presence of mainly foliation-parallel, 2–50-mm-thick yellow to greenish layers (Figure 3a). These layers consist of either ep (X_{Fe3+}=0.25–30) + Cal + Ttn + Qtz or Cpx ± Grt ± Pl (An$_{3–45}$) ± Ep (X_{Fe3+}=0.10–0.30) ± Cal + Qtz + Py ± Wo (Figure 4c, d; Table 4). Clinopyroxene- and garnet-bearing assemblages are confined to distances ≤300 m from the intrusive contact. Garnets have compositions of $Alm_{1–3}Sps_{0–2}Adr_{37–82}Grs_{60–11}$ (Figure 5c), and show micrometer-scale oscillatory zoning of varying grossular-andradite components (Figure 6). Clinopyroxenes have compositions of $Wo_{46–52}En_{18–42}Fs_{5–31}$ with Al_2O_3 contents of ≤ 2.50 wt % (Figure 5d).

At a distance of ~400 m from the intrusive contact (sample 482), former phyllites are still fine-grained (∅~75–150 μm), and comprise Chl (Mg# 0.45–0.49) + Ms (Si~3.05–3.14 cpfu) + Bt (Mg# 0.38–0.42; ti~0.15–0.21 cpfu) + Pl (An$_{0–5}$ & An$_{15–20}$) + Qtz ± And ± Ilm ± Tur ± Mnz (Figure 2; Tables 1 & 5). Muscovite and biotite locally overgrow the regional metamorphic foliation. A large scatter in muscovite compositions is probably caused by incomplete resetting during contact metamorphism. Approaching the intrusive contact, chlorite and muscovite disappear, and grain sizes locally increase up to 250 μm. At a distance ≤ 30 m (samples 481b and 531), 1- to 3-mm-thick discontinuous and undeformed leucosomes with microperthitic Kfs (X_{Or}~0.84–0.96) + Qtz ± Pl (An$_{0–5}$) have developed, which alternates with mesosomes comprising Bt (Mg#

0.38–0.47; Ti~0.08–0.25 cpfu) + Pl (An$_{17–35}$) + And ± Qtz ± Crn (Figures 3 & 4e, f; Table 5). Typically, an albitic seam is situated between leucosomes and melanosomes. Leucosomes have peraluminous, low-Ca and potassic granitic compositions. Andalusite occurs as xenoblastic grains with inclusions of biotite (Figure 4e), and is marginally replaced by muscovite (Si~3.05–3.09 cpfu) or margarite (X_{Ca}~0.80–0.84). Corundum is intergrown with K-feldspar and plagioclase, and is replaced by muscovite and diaspore (Figure 4f).

Carboniferous High-grade Tectono-metamorphic (Cenci) Unit

The Cenci unit underwent Carboniferous lower granulite-facies metamorphism (≥ 800 ºC, 0.7–0.8 GPa and 327–331 Ma BP; Topuz *et al.* 2004b) followed by pervasive sub- to greenschist-facies rehydration during exhumation (230–400 ºC, 0.1–0.3 Gpa and 310–315 Ma BP; Topuz & Altherr 2004), and bounds the western margin of the granodiorite. Within the contact aureole, the Cenci unit comprises mesocratic metapelitic gneisses and amphibolites, of which only one amphibolite sample (sample 467) has been studied herein. The immediate contact of the high-grade rocks with the intrusion cannot be observed due to poor outcrop conditions. Sample 467 displays a feeble foliation, and consists of calcic amphibole, Pl (An$_{92–97}$), Ilm (MnO≤3 wt. %), Py and secondary Chl (X_{Mg}~0.70–0.77). Similar to the metabasic lithologies in the Doğankavak subunit, amphibole has a patchy appearance caused by compositionally distinct domains ranging from actinolite to pargasite (Table 2; Figure 5a). Outside the contact aureole, the amphibolites are characterized by hornblendes with Al_2O_3 contents of 5–9 wt % and plagioclase (An$_{30–65}$), implying that the high-Al amphiboles and anorthitic plagioclases formed via contact-metamorphic overprinting. No epidote has been found in this unit; thus, it is unlike the metabasites of the Doğankavak unit.

Late Carboniferous Sedimentary Rocks

Late Carboniferous sedimentary rocks consist of siltstone, claystone and limestone, and are exposed at the northwestern and northern margins of the intrusion (e.g., Okay & Leven 1996; Çapkınoğlu 2003). These rocks are transformed into spotted phyllites (samples 528 and 529) at a distance of ~450 m from the intrusive

Table 3. Selected representative electron-microprobe analyses of epidote, chlorite, ilmenite, magnetite and titanite from metabasic lithologies, Saraycık contact aureole.

Sample	446A	446A	447	448	523	523	447	448	476	447	448	467	481c	446A	446B	447	481C	446A	446B	447	448	476	481c
Mineral	Ep	Ep	Ep	Ep	Ep	Ep	Chl	Chl	Chl	Ilm	Ilm	Ilm	Ilm	Mag	Mag	Mag	Mag	Ttn	Ttn	Ttn	Ttn	Ttn	Ttn
Analyse	9	88	53	7	2	22	34	67	122	77	48	63	51	60	16	75	5	8	21	4	8	1	2
SiO_2	37.55	38.90	37.37	38.03	37.26	37.94	25.67	27.70	25.45	0.05	0.04	0.02	0.00	0.02	0.07	0.01	0.01	30.34	30.65	30.77	30.40	30.21	30.41
TiO_2	0.10	0.00	0.04	0.03	0.14	0.08	0.00	0.07	0.10	50.63	50.73	51.19	48.62	0.03	0.15	0.40	0.08	39.02	38.67	38.32	38.28	37.39	35.67
Al_2O_3	23.59	29.88	22.43	23.33	22.75	27.75	18.20	20.56	20.68	0.00	0.00	0.00	0.00	0.05	0.13	0.15	0.06	0.69	1.00	1.04	0.84	1.49	1.91
Cr_2O_3	0.03	0.00	0.00	0.01	0.02	0.09	0.02	0.07	0.00	0.03	0.16	0.09	0.05	0.06	0.00	0.17	0.51	0.01	0.03	0.05	0.00	0.08	0.04
FeO	11.42	3.82	12.59	12.17	12.85	6.73	32.79	15.74	26.91	45.25	43.37	44.04	45.01	91.72	91.95	92.13	91.31	0.47	0.41	0.45	0.84	0.44	0.89
MnO	0.15	0.26	0.03	0.14	0.13	0.61	0.52	0.18	0.46	3.14	2.12	2.51	3.51	0.00	0.17	0.00	0.07	0.07	0.08	0.09	0.08	0.03	0.03
MgO	0.01	0.00	0.00	0.01	0.00	0.01	9.85	22.63	12.98	0.05	0.29	0.15	0.47	0.00	0.01	0.00	0.01	0.00	0.00	0.00	0.02	0.00	0.00
CaO	23.38	23.99	23.38	22.95	23.02	23.16	0.25	0.09	0.06	0.40	0.40	0.26	0.25	0.27	0.15	0.02	0.22	28.09	28.51	28.41	28.06	28.14	28.04
Na_2O	0.04	0.00	0.00	0.01	0.00	0.04	0.00	0.01	0.04	0.05	0.01	0.01	0.00	0.00	0.00	0.01	0.00	0.03	0.05	0.03	0.04	0.02	0.02
K_2O	0.00	0.00	0.00	0.01	0.03	0.01	0.02	0.04	0.13	0.00	0.00	0.00	0.00	0.00	0.00	0.00	0.01	0.02	0.01	0.00	0.03	0.00	0.00
Total	96.28	96.85	95.83	96.69	96.21	96.40	87.30	87.09	86.79	99.60	97.13	98.26	97.91	92.16	92.62	92.89	92.28	98.73	99.40	99.16	98.58	97.79	97.02

Cations on the basis of 12.5 oxygens (Ep), 14 oxygens (Chl); Normalized to 3 oxygens and 2 cations (Ilm), 4 oxygens and 3 oxygens (Mag), 5 oxygens and 3 cations (Ttn)

	446A	446A	447	448	523	523	447	448	476	447	448	467	481c	446A	446B	447	481C	446A	446B	447	448	476	481c
Si	2.998	3.014	3.007	3.020	2.988	2.983	2.844	2.787	2.740	0.001	0.001	0.001	0.000	0.001	0.003	0.001	0.000	1.002	1.005	1.011	1.006	1.006	1.020
Ti	0.006	0.000	0.002	0.002	0.009	0.004	0.000	0.005	0.008	0.961	0.987	0.986	0.935	0.001	0.004	0.012	0.002	0.969	0.954	0.947	0.952	0.936	0.900
Al	2.219	2.728	2.127	2.184	2.150	2.572	2.377	2.439	2.625	0.000	0.000	0.000	0.000	0.002	0.006	0.007	0.003	0.027	0.039	0.040	0.033	0.058	0.076
Cr	0.002	0.000	0.000	0.001	0.001	0.005	0.002	0.006	0.000	0.001	0.003	0.002	0.001	0.002	0.000	0.005	0.016	0.000	0.001	0.001	0.000	0.002	0.001
Fe^{3+}	0.763	0.248	0.848	0.808	0.862	0.443	0.000	0.000	0.000	0.077	0.020	0.025	0.128	1.993	1.980	1.964	1.977	0.013	0.011	0.012	0.023	0.012	0.025
Fe^{2+}	0.000	0.000	0.000	0.000	0.000	0.000	3.038	1.324	2.423	0.878	0.919	0.919	0.834	0.990	0.995	1.010	0.989	0.000	0.000	0.000	0.000	0.000	0.000
Mn	0.010	0.017	0.002	0.010	0.009	0.040	0.049	0.015	0.042	0.067	0.046	0.054	0.076	0.000	0.006	0.000	0.002	0.002	0.002	0.003	0.002	0.000	0.000
Mg	0.001	0.000	0.000	0.002	0.000	0.001	1.626	3.395	2.083	0.002	0.011	0.006	0.018	0.000	0.000	0.000	0.001	0.000	0.000	0.000	0.001	0.000	0.000
Ca	2.000	1.991	2.016	1.953	1.977	1.951	0.029	0.010	0.006	0.011	0.011	0.007	0.007	0.011	0.000	0.001	0.009	0.994	1.002	1.000	0.995	1.004	1.007
Na	0.005	0.000	0.000	0.002	0.000	0.007	0.000	0.001	0.009	0.002	0.000	0.000	0.000	0.000	0.000	0.001	0.000	0.002	0.003	0.002	0.003	0.001	0.001
K	0.000	0.000	0.000	0.001	0.003	0.001	0.002	0.005	0.018	0.000	0.000	0.000	0.000	0.000	0.000	0.000	0.001	0.001	0.000	0.000	0.001	0.000	0.000
X_{Fe3+}	0.26	0.08	0.29	0.27	0.29	0.15	-	-	-	-	-	-	-	-	-	-	-	-	-	-	-	-	-
Mg#	-	-	-	-	-	-	0.35	0.72	0.46	-	-	-	-	-	-	-	-	-	-	-	-	-	-

X_{Fe3+} $Fe^{3+}/(Al+Fe^{3+})$, Mg# $Mg/(Mg+Fe^{2+})$

Table 4. Selected representative electron-microprobe analyses of garnet, clinopyroxene and wollastonite from yellowish to brown layers in metabasic lithlogies, Saraycik contact aureole.

Sample	447	447	447	481C	481C	481C	523	523	523	446A	446A	446A	447	447	481C	481C	481C	523	523	447	447	447	447
Mineral	Grt	Grt	Grt	Grt	Grt	Grt	Grt	Grt	Grt	Cpx	Cpx	Cpx	Cpx	Cpx	Cpx	Cpx	Cpx	Cpx	Cpx	Wo	Wo	Wo	Wo
Analyse	32	46	115	43	44	45	55	59	64	86	87	76	1	7	1	30	40	56	27	98	99	104	108
SiO₂	37.96	36.87	36.05	35.183	36.779	35.76	36.20	36.09	37.448	50.69	51.52	51.39	50.03	50.80	50.99	51.42	50.27	50.56	50.97	51.56	51.65	51.70	51.72
TiO₂	0.84	1.46	0.01	0.46	0.47	0.50	2.19	0.44	0.70	0.06	0.24	0.19	0.03	0.02	0.05	0.29	0.09	0.01	0.04	0.00	0.00	0.02	0.00
Al₂O₃	13.39	9.60	3.53	3.63	10.90	5.42	7.95	5.27	12.37	1.45	2.23	2.11	0.40	0.41	0.88	2.34	0.74	0.23	0.44	0.03	0.04	0.02	0.01
Cr₂O₃	0.00	0.09	0.04	0.09	0.00	0.11	0.08	0.01	0.03	0.00	0.00	0.00	0.07	0.03	0.05	0.08	0.00	0.01	0.05	0.02	0.00	0.00	0.06
FeO	12.13	15.91	23.62	24.81	15.15	22.54	16.43	21.21	12.25	14.65	8.90	7.95	19.10	16.88	13.51	6.21	15.27	16.75	14.33	0.12	0.28	0.55	0.14
MnO	0.25	0.53	0.17	1.30	0.98	0.90	0.25	0.10	0.21	0.41	0.57	0.51	0.70	0.83	0.51	0.28	0.74	0.66	0.65	0.24	0.25	0.24	0.35
MgO	0.02	0.01	0.00	0.03	0.00	0.08	0.00	0.01	0.02	8.55	12.07	13.01	5.77	7.24	10.52	14.37	8.97	7.11	8.64	0.00	0.00	0.00	0.00
CaO	34.79	33.98	33.90	31.00	33.83	32.20	34.26	33.45	34.59	23.42	23.83	24.41	23.55	23.84	23.74	24.64	23.11	23.39	23.90	47.63	47.50	47.42	47.55
Na₂O	0.03	0.02	0.03	0.00	0.00	0.00	0.01	0.02	0.02	0.27	0.32	0.26	0.14	0.19	0.33	0.25	0.35	0.10	0.15	0.02	0.01	0.02	0.00
K₂O	0.00	0.00	0.01	0.00	0.01	0.03	0.00	0.01	0.01	0.02	0.03	0.02	0.01	0.00	0.01	0.00	0.00	0.02	0.02	0.01	0.01	0.00	0.01
Total	99.41	98.47	97.37	96.49	98.12	97.54	97.37	96.61	97.64	99.53	99.70	99.86	99.78	100.24	100.57	99.88	99.52	98.85	99.19	99.61	99.75	99.97	99.84

Normalized to 12 oxygens and 8 cations (Grt) and 6 oxygens and 4 cations (Cpx, Wol)

	447 Grt 32	447 Grt 46	447 Grt 115	481C Grt 43	481C Grt 44	481C Grt 45	523 Grt 55	523 Grt 59	523 Grt 64	446A Cpx 86	446A Cpx 87	446A Cpx 76	447 Cpx 1	447 Cpx 7	481C Cpx 1	481C Cpx 30	481C Cpx 40	523 Cpx 56	523 Cpx 27	447 Wo 98	447 Wo 99	447 Wo 104	447 Wo 108
Si	2.974	2.962	2.993	2.96	2.95	2.95	2.956	2.996	2.992	1.960	1.936	1.918	1.976	1.976	1.932	1.901	1.945	1.996	1.982	2.002	2.003	2.002	2.003
Ti	0.050	0.088	0.001	0.029	0.029	0.031	0.134	0.028	0.042	0.002	0.007	0.005	0.001	0.001	0.001	0.008	0.003	0.000	0.001	0.000	0.000	0.001	0.000
Al	1.236	0.909	0.345	0.360	1.031	0.528	0.766	0.516	1.164	0.066	0.099	0.093	0.019	0.019	0.039	0.102	0.034	0.011	0.020	0.001	0.002	0.001	0.000
Cr	0.000	0.006	0.003	0.006	0.000	0.007	0.005	0.001	0.002	0.000	0.000	0.000	0.002	0.001	0.001	0.002	0.000	0.000	0.002	0.001	0.000	0.000	0.002
Fe³⁺	0.721	0.989	1.640	1.648	1.014	1.499	1.049	1.439	0.770	0.031	0.039	0.081	0.035	0.041	0.118	0.096	0.098	0.004	0.025	0.000	0.000	0.000	0.000
Fe²⁺	0.074	0.080	0.000	0.099	0.002	0.057	0.073	0.033	0.049	0.443	0.240	0.168	0.596	0.508	0.310	0.096	0.396	0.549	0.441	0.004	0.009	0.018	0.004
Mn	0.016	0.036	0.012	0.092	0.067	0.063	0.017	0.007	0.014	0.014	0.018	0.016	0.023	0.027	0.016	0.009	0.024	0.022	0.021	0.008	0.008	0.008	0.012
Mg	0.002	0.002	0.000	0.003	0.000	0.010	0.000	0.001	0.002	0.493	0.676	0.724	0.340	0.420	0.594	0.792	0.517	0.418	0.501	0.000	0.000	0.000	0.000
Ca	2.921	2.925	3.016	2.797	2.907	2.849	2.998	2.975	2.961	0.970	0.959	0.976	0.997	0.993	0.964	0.976	0.958	0.990	0.995	1.981	1.974	1.967	1.974
Na	0.005	0.004	0.005	0.000	0.001	0.000	0.001	0.003	0.003	0.020	0.023	0.019	0.010	0.014	0.024	0.018	0.026	0.008	0.011	0.001	0.000	0.001	0.000
K	0.000	0.000	0.001	0.000	0.001	0.003	0.000	0.001	0.001	0.001	0.001	0.001	0.000	0.000	0.000	0.000	0.000	0.001	0.001	0.000	0.001	0.000	0.001
Total	8.000	8.000	8.015	8.000	8.000	8.000	8.000	8.000	8.000	4.000	4.000	4.000	4.000	4.000	4.000	4.000	4.000	4.000	4.000	3.998	3.997	3.998	3.996
Mg#	0.02	0.02	0.00	0.03	0.00	0.14	0.00	0.04	0.04	0.53	0.74	0.81	0.36	0.45	0.66	0.89	0.57	0.43	0.53	-	-	-	-
X$_{Alm}$	0.02	0.03	0.00	0.03	0.00	0.02	0.02	0.01	0.02	-	-	-	-	-	-	-	-	-	-	-	-	-	-
X$_{Pyp}$	0.00	0.00	0.00	0.00	0.00	0.00	0.00	0.00	0.00	-	-	-	-	-	-	-	-	-	-	-	-	-	-
X$_{Sps}$	0.01	0.01	0.00	0.03	0.02	0.02	0.01	0.00	0.00	-	-	-	-	-	-	-	-	-	-	-	-	-	-
X$_{Adr}$	0.37	0.52	0.83	0.82	0.50	0.74	0.58	0.74	0.40	-	-	-	-	-	-	-	-	-	-	-	-	-	-
X$_{Grs}$	0.60	0.44	0.17	0.11	0.48	0.22	0.39	0.25	0.58	-	-	-	-	-	-	-	-	-	-	-	-	-	-

Mg# Mg/(Mg+Fe²⁺)

Table 5. Selected representative electron-microprobe analyses of biotite, plagioclase, K-feldspar, spinel, muscovite, chlorite, ilmenite and margarite from pelitic lithologies, Saraycık contact aureole.

Sample	482	482	531	531	545	545	545	545	482	531	531	545	545	531	545	545	482	531	482	482	531	545	531	531
Mineral	Bt	Bt	Bt	Bt	Bt	Bt	Bt	Bt	Pl	Pl	Pl	Pl	Pl	Kfs	Crd	Spl	Ms	Ms	Chl	Chl	Ilm	Ilm	Mrg	Mrg
Analyse	1	6	1	89	5	8	161	224	43	3	9	2	194	16	13	221	7	2	29	38	57	54	81	82
SiO_2	34.20	34.56	34.23	35.14	35.66	36.07	35.52	34.34	63.63	59.17	68.55	59.27	62.27	65.25	47.88	0.04	45.72	46.97	24.99	24.02	0.09	0.05	30.44	30.37
TiO_2	3.41	2.58	1.37	4.24	2.20	2.64	2.75	0.83	0.03	0.00	0.00	0.00	0.00	0.00	0.02	7.92	0.07	0.43	0.23	0.27	52.20	47.72	0.06	0.07
Al_2O_3	17.46	18.75	19.53	15.75	18.94	19.60	17.80	21.08	21.87	25.70	20.40	24.60	23.16	18.61	32.67	53.69	32.71	35.35	21.20	21.49	0.00	0.00	49.75	49.84
Cr_2O_3	0.30	0.26	0.06	0.15	0.00	0.01	0.00	0.00	0.01	0.00	0.00	0.01	0.00	0.07	0.03	0.00	0.05	0.12	0.32	0.10	0.01	0.08	0.02	0.06
FeO	20.37	19.32	19.96	21.21	14.47	14.34	17.03	17.04	0.73	0.18	0.04	0.04	0.09	0.04	7.95	33.92	2.82	2.50	25.56	26.82	34.57	48.26	0.45	0.60
MnO	0.12	0.08	0.77	0.46	0.08	0.19	0.08	0.19	0.08	0.07	0.00	0.09	0.00	0.00	0.28	0.25	0.00	0.03	0.17	0.12	10.56	2.58	0.00	0.03
MgO	7.74	7.86	9.52	8.42	12.10	12.05	11.91	10.93	0.01	0.00	0.01	0.01	0.00	0.01	7.54	2.04	2.01	0.63	13.52	12.45	0.00	0.00	0.15	0.20
CaO	0.00	0.04	0.03	0.04	0.02	0.00	0.02	0.08	3.40	7.33	0.67	6.22	5.07	0.07	0.05	0.03	0.00	0.00	0.01	0.00	0.00	0.03	11.70	11.50
Na_2O	0.15	0.14	0.10	0.08	0.16	0.14	0.12	0.12	9.68	7.50	11.26	7.98	8.55	1.76	0.48	0.00	0.49	0.37	0.00	0.02	0.00	0.01	1.22	1.36
K_2O	9.26	8.93	9.54	9.50	9.55	9.14	9.08	9.50	0.19	0.17	0.20	0.08	0.19	14.19	0.01	0.00	9.96	10.21	0.08	0.05	0.22	0.02	0.28	0.08
ZnO	n.a.	n.a.	n.a.	n.a.	n.a.	n.a.	n.a.	n.a.	n.a.	n.a.	n.a.	n.a.	n.a.	n.a.	n.a.	1.68	n.a.	n.a.	n.a.	n.a.	n.a.	n.a.	n.a.	n.a.
Total	93.00	92.50	95.09	94.99	93.19	94.17	94.33	93.46	99.63	100.12	101.12	98.28	99.56	100.01	96.90	99.89	93.83	96.61	86.06	85.34	97.72	98.74	94.07	94.39

Cations on the basis of 11 oxygens (Bt, Ms and Mrg), 8 oxygens (Pl, Kfs), 18 oxygens (Crd), 14 oxygens (Chl); N. to 4 oxygens and 3 cations (Spl), 3 oxygens and 2 cations (Ilm)

	482	482	531	531	545	545	545	545	482	531	531	545	545	531	545	545	482	531	482	482	531	545	531	531
Si	2.697	2.710	2.636	2.731	2.713	2.702	2.701	2.620	2.826	2.640	2.965	2.685	2.777	2.993	5.004	0.001	3.112	3.091	2.693	2.633	0.002	0.001	2.049	2.043
Ti	0.202	0.152	0.080	0.248	0.126	0.149	0.157	0.048	0.001	0.000	0.000	0.000	0.000	0.000	0.001	0.175	0.003	0.021	0.018	0.022	1.008	0.913	0.003	0.004
Al	1.623	1.733	1.772	1.443	1.698	1.730	1.595	1.896	1.145	1.351	1.040	1.313	1.217	1.006	4.024	1.858	2.721	2.742	2.693	2.777	0.000	0.000	3.945	3.945
Cr	0.019	0.016	0.004	0.009	0.000	0.001	0.000	0.000	0.000	0.007	0.001	0.001	0.000	0.003	0.003	0.000	0.003	0.006	0.027	0.009	0.000	0.002	0.001	0.003
Fe^{3+}	0.000	0.000	0.000	0.000	0.000	0.000	0.000	0.000	0.000	0.000	0.000	0.000	0.000	0.002	0.000	0.000	0.000	0.000	0.000	0.000	0.000	0.171	0.000	0.000
Fe^{2+}	1.343	1.267	1.285	1.379	0.921	0.898	1.083	1.087	0.027	0.007	0.001	0.001	0.000	0.000	0.695	0.833	0.160	0.138	2.304	2.459	0.743	0.855	0.025	0.034
Mn	0.008	0.005	0.050	0.030	0.005	0.012	0.005	0.012	0.003	0.002	0.000	0.003	0.000	0.000	0.025	0.006	0.000	0.001	0.015	0.011	0.230	0.056	0.000	0.002
Mg	0.910	0.919	1.092	0.976	1.372	1.346	1.350	1.243	0.001	0.000	0.000	0.000	0.000	0.001	1.175	0.089	0.204	0.062	2.172	2.035	0.003	0.000	0.015	0.020
Ca	0.000	0.003	0.002	0.003	0.002	0.000	0.002	0.007	0.162	0.351	0.031	0.302	0.242	0.004	0.006	0.001	0.000	0.000	0.001	0.000	0.000	0.001	0.844	0.829
Na	0.023	0.021	0.016	0.013	0.023	0.020	0.018	0.018	0.834	0.649	0.944	0.701	0.739	0.157	0.097	0.000	0.064	0.047	0.000	0.005	0.000	0.000	0.160	0.177
K	0.931	0.894	0.937	0.942	0.927	0.874	0.881	0.925	0.011	0.009	0.011	0.005	0.011	0.830	0.001	0.000	0.865	0.857	0.011	0.007	0.007	0.001	0.024	0.007
Zn																0.036								
X_{Mg}	0.40	0.42	0.46	0.41	0.60	0.60	0.55	0.53							0.63	0.10			0.49	0.45				
X_{Na}	0.02	0.02	0.02	0.01	0.02	0.02	0.02	0.02	0.83	0.64	0.96	0.70	0.75	0.16			0.07	0.05					0.16	0.17
X_{Ca}	0.00	0.00	0.00	0.00	0.00	0.00	0.00	0.01	0.16	0.35	0.03	0.30	0.24	0.00			0.00	0.00					0.82	0.82
X_K	0.98	0.97	0.98	0.98	0.97	0.98	0.98	0.97	0.01	0.01	0.01	0.00	0.01	0.84			0.93	0.95					0.02	0.01

n.a. = not analyzed. N. = normalized, X_{Mg} Mg/(Mg+Fe), X_{Na} Na/(Na+Ca+K), X_{Ca} Ca/(Na+Ca+K), X_K K/(Na+Ca+K)

contact, and into biotite felses (samples 544b and 545) near the intrusive contact (Figure 2). Spotted phyllites are fine-grained (20–40 µm), and comprise Ab/Ande (An_{0-4} and An_{15-20}), Qtz, Ms (Si~3.08–3.20 cpfu), Bt (X_{Mg}~0.45–0.50; Ti~0.08–0.09 cpfu), Chl (X_{Mg}~0.40–0.49), Tur and secondary Illite (Ill). Andesine is confined to cracks in the albite grains. Spots (up to 600 µm) are made up of mineral aggregates such as Pl (An_{0-4} and An_{15-20}), Qtz, Ms, Bt, Tur and Ill. Illite overgrows the other phases, suggesting that it has replaced the porphyroblast-forming mineral. Biotite felses are mostly massive and dark-coloured, and comprise Pl (An_{2-42}), Bt (X_{Mg}~0.53–0.63; Ti~0.05–0.22 cpfu), Qtz, minor Kfs (X_{Kfs}~0.85–0.95), and secondary Ms and Chl (Table 5). Plagioclases in a single thin section display a large compositional variation (An_{2-42}), and occur in two texturally different types, namely (a) inclusion-rich porphyroblasts (Ø~200–3000 µm; An_{2-42}) and (b) finer-grained matrix plagioclases (Ø~30–200 µm; An_{2-12}) intergrown with biotite (Figure 4g). Plagioclase porphyroblasts contain fine-grained inclusions of Bt (X_{Mg}~0.53; Ti~0.05 cpfu), Sil, Crd (X_{Mg}~0.62), Spl (X_{Mg}~0.10; Ti~0.18 cpfu; Zn~0.04 cpfu), Crn and Kfs (X_{Kfs}~0.85–0.92) (Figure 4h).

P–T Conditions of Contact Metamorphism

The extent of disequilibrium in the Saraycık aureole makes it difficult to determine contact metamorphic conditions. Metabasic lithologies show relatively complex textural and compositional phase relations, and are, therefore, of little use in determining the contact metamorphic *P–T* conditions (cf. the section "Petrography and Mineral Compositions"). Metapelitic lithologies display relatively simple phase and compositional relationships. Hence, microdomains in the metapelites, which contain P- and T-sensitive mineral assemblages and show no obvious sign of disequilibrium, were selected for the *P–T* estimates.

Pressure Estimates

The coexistence of andalusite, corundum und K-feldspar and the absence of primary muscovite in the melanosomes of samples 481 and 531 (Figure 4f) indicate that contact metamorphism occurred above the upper stability of muscovite within the andalusite stability field. According to Holdaway (1971) and Pattison

(1992), for a_{H2O}=1 in quartz-bearing rocks, the intersection of the muscovite upper thermal limit with the andalusite-sillimanite phase boundary yields maximum pressures of 0.18 and 0.28 Gpa, respectively (Figure 7). Reduced water activities would shift the intersection to lower temperatures and higher pressures. Insofar as only Pattison's version allows for andalusite + melt stability, the pressure value, 0.28 GPa, is regarded as the maximum pressure constraint. Minimum pressures are not constrained. The maximum pressure constraints are consistent with those (0.21±0.05 GPa; ~5–8 km) obtained from Al-in-hornblende barometry on the granodiorite itself (Topuz *et al.* 2005). In addition, the absence of garnet in the pelitic bulk compositions and evidence for partial melting in the andalusite stability field (see Discussion, below) are also strong arguments for relatively low-pressures; that is, shallow emplacement depths.

Temperature Estimates

Temperatures at different points within the contact aureole are estimated by means of the calculated position of relevant mineral equilibria using the Thermocalc v3.21 software (Holland & Powell 1998). Given the relatively small size of the intrusion and the absence of any indication of post-contact metamorphic tilting, it is assumed that the peak temperatures at each point were attained at roughly the same pressure (0.21±0.05 Gpa) in the contact aureole.

The mineral assemblage "chlorite + biotite + muscovite + plagioclase ± andalusite + quartz" in an andalusite-bearing microdomain of a former phyllite (sample 482; ~400 m further from the granodiorite contact) allows rough temperature constraints. Based on the absence of staurolite, the following reaction can be used to ascertain the lowest temperature constraints:

$$St + Chl + Ms = And + Bt + H_2O \qquad (1)$$
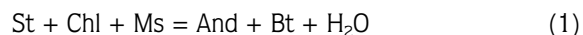
The reaction is located at 487 ºC at 0.2 GPa, respectively, for a_{Mg-St}= 1; a_{Ms}= 0.70; a_{Clin}= 0.02, a_{And}=1, a_{Phl} =0.0215 and a_{H2O}=1 whereby the activities of muscovite, clinochlore in chlorite, and phlogopite in biotite are calculated by the aX software of T.J.B. Holland (http://www.esc.cam.ac.uk/astaff/holland). At a_{H2O}= 0.5,

the reaction shifts to 430 °C at 0.2 Gpa. An additional constraint is provided by the following reaction

$$Ms + Chl = Qtz + And + Bt + H_2O \qquad (2)$$

The reactions (2) lie at 517 °C at 0.2 GPa for a_{Ms}= 0.70, a_{Clin}= 0.02, a_{Qtz}=1, a_{And}=1, a_{H2O}= 1). Reduced water activity (e.g., a_{H2O}= 0.5) shifts the reactions to lower temperatures, i.e., 430 °C. Given the unknown absolute value of water activity and uncertainties in the calculations, it may be concluded that the temperatures attained at the site of sample 482 were ~430–520 °C at 0.2 GPa.

The presence of andalusite, corundum and K-feldspar and the absence of primary muscovite in samples 481 and 531 (~30–10 m from the intrusive contact) can be used to place the minimum temperature constraints near the intrusive contact via the following reactions:

$$Ms + Qtz = And + Kfs + H_2O \qquad (3)$$
$$Ms = Crn + Kfs + H_2O \qquad (4)$$
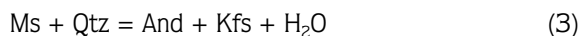
At 0.2 Gpa and a_{H2O}=1, these reactions constrain metamorphic temperatures to over 590 and 630 °C, respectively (Figure 7). The occurrence of corundum in contact-metamorphic pelites was also reported by Rosing *et al.* (1987) and Fukuyama *et al.* (2004). The andalusite-sillimanite phase boundary provides the maximum temperature constraint (730 °C at 0.2 Gpa) for this assemblage. Altogether, the temperatures must have been between 630 and 730 °C.

Inclusions of spinel, corundum, sillimanite, K-feldspar and cordierite in plagioclase porphyroblasts within sample 545 can be accounted for by the following reactions (e.g., Pattison & Harte 1997):

$$Bt + Sil + Qtz = Crd + Kfs + melt \qquad (5)$$
$$Bt + Sil = Spl + Crn + Crd + Kfs + H_2O/melt \qquad (6)$$
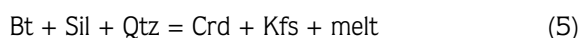
The presence of sillimanite requires minimum temperatures of 730±20 °C at 0.2 Gpa (Figure 5). Maximum temperatures can be constrained, albeit poorly,

by the absence of orthopyroxene in both metapelitic and metabasic lithologies to ~800 °C (Figure 7).

The formation of secondary phases such as margarite and diaspore in samples 481 and 531 can be accounted for by the interaction of lower-temperature fluids during retrograde evolution according to the following reactions:

$$Crn + H_2O = 2\ Dsp \qquad (7)$$
$$An\ (in\ Pl) + Crn + H_2O = Mrg \qquad (8)$$
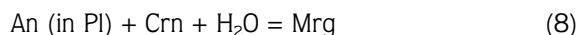
These reactions occur at temperatures below 390 and 500 °C at 0.2 GPa, respectively, if unit activities are assumed.

To summarize, the estimated peak temperatures range from ~430–520 °C at ~400 m away from the granodiorite contact to over 730 °C immediate adjacent to the intrusive contact. During the waning stages of contact metamorphism, primary assemblages were partially hydrated at temperatures below 500 °C.

Temperatures of Country Rocks Prior to Emplacement

The temperatures of the intruding Saraycık magmas were estimated by apatite saturation temperatures, as ~900–950 °C (Topuz *et al.* 2005). At what temperatures were the country rocks prior to the intrusion of the granodiorite? An aureole pressure of 0.21 Gpa gives a depth estimate of ~7 km for a nominal density of 2800 kg/m³. If a high regional geothermal gradient such as 30 °C/km is assumed, this would yield an ambient temperature of 200–210 °C, regarded as an upper limit.

Discussion

Phase Relations and Foliation-parallel Layers Within Metabasic Lithologies

Experimental work on metabasites has revealed that, with increasing temperature at a constant pressure, chlorite, epidote + quartz and titanite disappear, and clinopyroxene, orthopyroxene and olivine appear sequentially dependent on P, T and X (Spear 1981, 1993; Moody *et al.* 1983; Apted & Liou 1983; Maruyama *et al.* 1983; Figure 5). Increasing oxygen fugacity stabilizes titanite and epidote to higher temperatures, and chlorite

and clinopyroxene to lower temperatures. In all the metabasites, titanite is present even in samples (e.g., 481 ºC) near the intrusion contact, implying that the upper temperature limit of titanite is not exceeded. Primary chlorite is confined to the outer domain of the contact aureole (samples 448 and 476, $\geq$ 500 m from the intrusive contact). The upper T limit of chlorite in the QFM buffer is given as 550 ºC (Apted & Liou 1983). Clinopyroxene is confined to the yellow to brown layers within the metabasites. Therefore, their presence cannot be taken as evidence for the appearance of clinopyroxene in the metabasic lithologies.

The mineral assemblages of yellow to brown layers within the metabasites show close correspondence to those of calcic skarns (Evans 1998, p. 157–170). Inasmuch as the layers are confined to the contact aureole, and locally cross-cut the regional metamorphic foliation, they must be genetically related to the granodiorite intrusion and should be regarded as the pathways for reactive fluids during contact metamorphism. There are three possible sources for these fluids: (a) the crystallizing Saraycık granodiorite at depth; (b) meteoric water heated by the granodiorite intrusion; and (c) dehydration of metabasic or metapelitic lithologies due to contact metamorphism. Given the data presently available, all three possibilities are equally likely. Thus, a detailed stable-isotope study would be highly desirable. Insofar as the layers are mostly parallel to the metabasic layers and locally cross-cut the foliation, fluid flow was apparently localized to foliation planes. Similar layers, which have been related to infiltration of high-temperature fluids, have been described from the Sanbagawa metamorphic belt (e.g., Sakakibara & Isono 1996).

Evidence for Disequilibrium and Its Implications

Several thin-section-scale textural and compositional characteristics point toward widespread disequilibrium in the Saraycık contact aureole; these are (1) coexistence of compositionally distinct plagioclase and amphibole adjacent to one another (Figure 4a, b); (2) wide compositional variation of some minerals, such as muscovite, plagioclase, garnet and clinopyroxene (Figure 5); and (3) oscillatory zoning in garnet (Figures 6). The occurrence of compositionally distinct amphibole and plagioclase next to each other, and oscillatory zoning in

garnet are confined to metabasic lithologies. In metapelitic lithologies, disequilibrium is reflected by large compositional variation in muscovites and plagioclases. In both lithologies, the amount of the disequilibrium shows no unambiguous relationship to the intrusive contact. Protoliths of the contact-metamorphic rocks had widely different original states in terms of grain size and mineral content. In general, dry and coarse-grained rocks are less likely to equilibrate to contact-metamorphic conditions, while fine-grained lithologies such as siltstones would react relatively quickly (e.g., Wheeler *et al.* 2004). Biotite felses derived from the former siltstones contain plagioclases with An_{2-42} near the intrusion, suggesting that disequilibrium is not limited to coarse-grained metabasites, but also occurs in fine-grained ones.

Oscillations in garnet zoning, defined by varying grossular and andradite components, is a typical characteristic of garnets in the Saraycık contact aureole, similar to other shallow contact aureoles (Clechenko & Valley 2003 and references therein). Oscillatory zones have predominantly straight boundaries (Figure 6). Local resorption is observed along oscillatory zone boundaries, suggesting that dissolution and growth were involved in the formation of these compositional discontinuities, and that the euhedral shapes of the former garnet layers were simply retained, as suggested by García-Casco *et al.* (2002). These compositional fluctuations in a single garnet grain suggest temporal variation in one of the intensive parameters, such as P, T and X (or a combination thereof) during the course of garnet growth. The short timescales for contact metamorphism, in general, suggest that pressure change during the course of contact metamorphism is not likely. Therefore, the main factors in the formation of oscillatory zoning in garnet are tentatively suggested to be temporal fluctuations of T and/or fluid composition during the time of garnet growth. Oscillatory zoning in garnets from the wollastonite skarn of the Adirondack Mountains, New York, has been ascribed to fluid-system variability caused by temporal or spatial mixing of magmatic and meteoric fluids (Clechenko & Valley 2003), and oscillatory zoning in eclogitic garnets from a serpentinite mélange in Cuba has been interpreted in terms of subtle fluctuations in P-T conditions (García-Casco *et al.* 2002).

In summary, all of these textural characteristics suggest that thin-section-scale disequilibrium in the rocks of the Saraycık contact aureole is not only caused by the
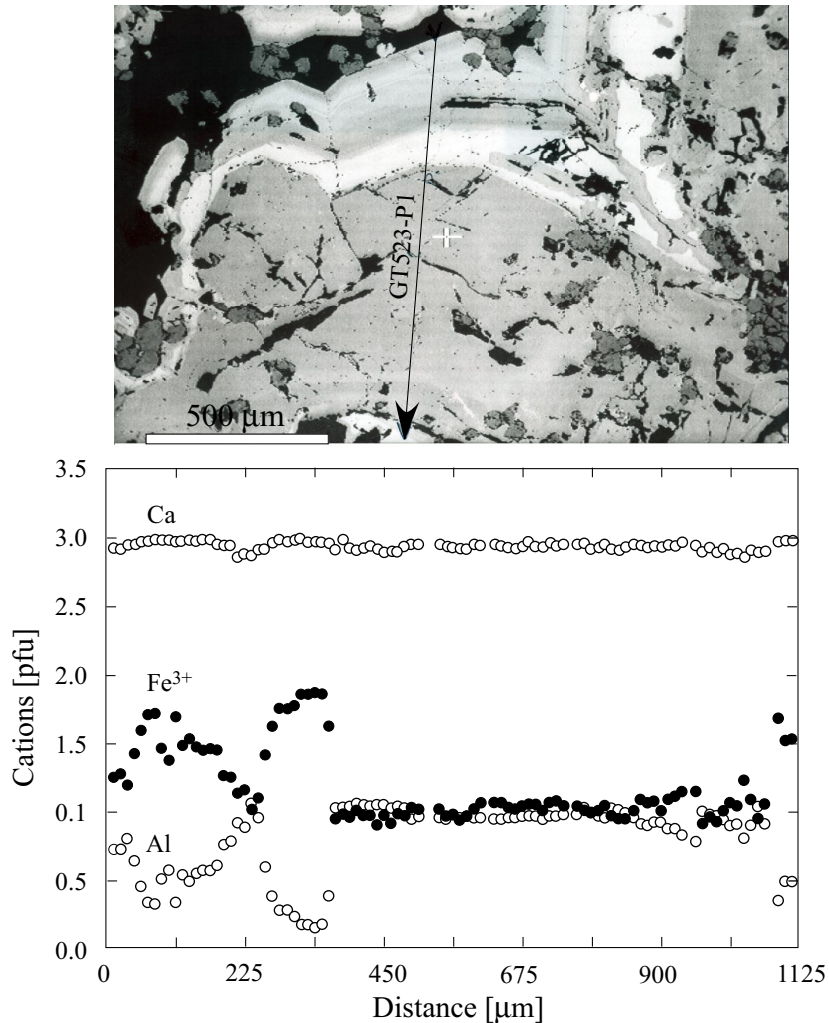
Figure 6. (a) Back-scattered electron image of part of a garnet with oscillatory zoning. Bright zones represent andradite-rich zones; (b) Compositional profile in terms of Ca, Fe^{3+} and Al along the line shown in (a).

presence of relict minerals from the pre-contact-metamorphic stage, but also, more importantly, by the temporal variation in intensive parameters, such as T and/or X (fluid composition), during contact metamorphism. The present level of data does not allow finer resolution of these intensive parameters.

Partial Melting within the Andalusite Stability Field

Microtextural characteristics in the leucosomes, such as coarse grain sizes relative to the melanosomes and the locally idiomorphic form of the leucosome minerals, suggest crystallization from a melt phase (Figures 3b & 4e). The absence of obvious cross-cutting relations points to local derivation of the partial melts. Therefore, equilibrium among the leucosomes, partial melts and andalusites may be assumed. According to Pattison (1992), the location of the And = Sil polymorphic reaction boundary allows for an andalusite + melt stability field below 0.26 GPa, while the work of Holdaway (1971) shows no intersection of this boundary with the wet solidus of granites or pelites (Figure 7). The
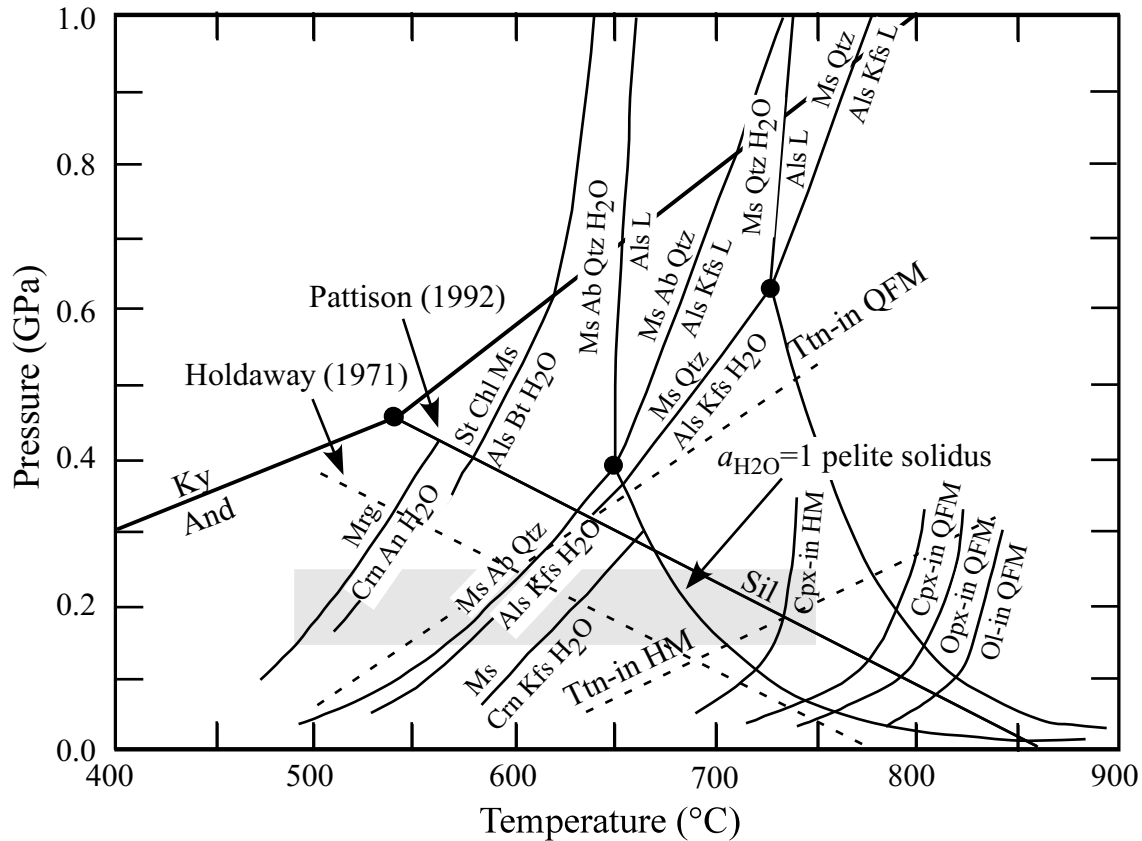
Figure 7. Pressure-temperature (*P–T*) diagram illustrating locations of the relevant reactions. Locations of the muscovite and margarite terminal reactions are calculated by Thermocalc software v3.02 (Holland & Powell 1997). Ttn-in, Cpx-in, Opx-in and Ol-in reactions are taken from Spear (1981). HM and QFM are hematite-magnetite and quartz-fayalite-magnetite buffers, respectively.

presence of melt inclusions in andalusite of volcanic rocks (Cesare *et al.* 2003), the presence of euhedral crystals of andalusite in some glassy felsic volcanic rocks, and the occurrence of euhedral andalusite crystals in granitic and anatectic rocks suggest an overlap of the stability fields for andalusite and silicate melt (Clarke *et al.* 2005 and references therein). High concentrations of Be, B, Li and Al_2O_3 have the effect of lowering the solidus of haplogranites (Johannes & Holz 1996; Clarke *et al.* 2005 and references therein). The present level of data does not allow complete assessment of these effects, but this paper does document another occurrence of andalusite in contact-metamorphic anatectic rocks.

Conclusions

The emplacement of the 52 Ma Saraycık granodiorite into cool (≤210 °C) country rocks – comprising a variety of tectonically juxtaposed lithologies – resulted in the development of a 0.8–1-km-wide contact metamorphic aureole. Pressures during contact metamorphism are estimated to have been 0.21±0.05 GPa, corresponding to depths of ~5–8 km. Peak temperatures during peak contact metamorphism ranged from 430–520 °C in the outer domains (~400 m) to ≥730 °C at the intrusive contact. Partial melting is confined to pelitic lithologies at distances ≤ 30 m from the igneous contact and occurred in the stability fields of both andalusite and sillimanite. Melting in the andalusite stability field probably occurred by wet-melting, and leucosome compositions correspond to peraluminous, low-Ca, potassic granites. Prograde mineral assemblages were locally overprinted due to fluid influx at temperatures below 500 °C. Within the metabasic lithologies, mainly foliation-parallel layers with skarn mineralogy have developed as a consequence of the interaction of chemically reactive fluids with host rocks.

Acknowledgements

References

APTED, M.J. & LIOU, J.G. 1983. Phase relations among greenschist, epidote amphibolite, and amphibolite in a basaltic system. *American Journal of Science* 283-A, 328–354.

ASLAN, Z. 2005. Petrography and petrology of the calc-alkaline Sarıhan granodiorite (NE Turkey): an example of magma mingling and mixing. *Turkish Journal of Earth Sciences* 14, 185–207.

BOZTUĞ, D., JONCKHEERE, R., WAGNER, G.A. & YEĞINGIL, Z. 2004. Slow Senonian and fast Palaeocene–Early Eocene uplift of the granitoids in the central eastern Pontides, Turkey: apatite fission-track results. *Tectonophysics* 382, 213–228.

ÇAPKINOĞLU, S. 2003. First records of conodonts from "the Permo–Carboniferous of Demirözü" (Bayburt), eastern Pontides, NE Turkey. *Turkish Journal of Earth Sciences* 12, 199–207.

CESARE, B., MARCHESI, C., HERMANN, J. & GOMEZ-PUGNAIRE, M.T. 2003. Primary melt inclusions in the andalusite from anatectic graphitic metapelites: implications for the position of the Al_2SiO_5 triple point. *Geology* 7, 573–576.

CLARKE, D.B., DORAIS, M., BARBARIN, B., BARKER, D., CESARE, B., CLARKE, G., EL BAGHDADI, M., ERDMANN, S., FORSTER, H.J., GAETA, M., GOTTESMANN, B., JAMIESON, R.A., KONTAK, D.J., KOLLER, F., GOMES, C.L., LONDON, D., MORGAN, G.B., NEVES, L.J.P.F., PATTISON, D.R.M., PEREIRA, A.J.S.C., PICHAVANT, M., RAPELA, C.W., RENNO, A.D., RICHARDS, S., ROBERTS, M., ROTTURA, A., SAAVEDRA, J., SIAL, A.N., TOSELLI, A.J., UGIDOS, J.M., UHER, P., VILLASECA, C., VISONA, D., WHITNEY, D.L., WILLIAMSON, B. & WOODARD, H.H. 2005. Occurrence and origin of andalusite in peraluminous felsic igneous rocks. *Journal of Petrology* 46, 441–472.

CLECHENKO, C.C. & VALLEY, J.W. 2003. Oscillatory zoning in garnet from the Willsboro wollastonite skarn, Adirondack Mts, New York: a record of shallow hydrothermal processes preserved in a granulite facies terrane. *Journal of Metamorphic Geology* 21, 771–784.

DROOP, G.T.R., CLEMENS, J.D. & DALRYMPLE D.J. 2003. Processes and conditions during contact anatexis, melt escape and restite formation: the Huntly gabbro complex, NE Scotland. *Journal of Petrology* 44, 995–1029.

EVANS, A.M. 1998. *Ore Geology and Industrial Minerals: An Introduction* (3rd edition). Blackwell Science, Tokyo.

GARCÍA-CASCO, A., TORRES-ROLDÁN, R.L., MILLÁN, G., MONIÉ, P. & SCHNEIDER, J. 2002. Oscillatory zoning in eclogitic garnet and amphibole, Northern Serpentinite Mélange, Cuba: a record of tectonic instability during subduction? *Journal of Metamorphic Geology* 20, 581–591.

FUKUYAMA, M., URATA, K. & NISHIYAMA, T. 2004. Geology and petrology of the Hirao Limestone and Tawaga metamorphic rocks – with special reference to contact metamorphism by Cretaceous granodiorite. *Journal of Mineralogical and Petrological Science* 99, 25–41.

HOLDAWAY, M.J. 1971. Stability of andalusite and Al_2SiO_5 phase diagram. *American Journal of Science* 271, 97–131.

HOLLAND, T.J.B. & POWELL, R. 1998. An internally consistent thermodynamic data set for phases of petrological interest. *Journal of Metamorphic Geology* 16, 309–343.

JOHANNES, W. & HOLTZ, E. 1996. *Petrogenesis and Experimental Petrology of Granitic Rocks.* Springer Verlag, Berlin.

KARSLI, O., AYDIN, F. & SADIKLAR, M.B. 2004. Magma interaction recorded in plagioclase zoning in granitoid systems, Zigana Granitoid, Eastern Pontides, Turkey. *Turkish Journal of Earth Sciences* 13, 287–306.

KERRICK, D.M. 1991. Overview of contact metamorphism. *In*: KERRICK, D.M. (ed), *Contact Metamorphism*. Mineralogical Society of America, Reviews in Mineralogy 26, 1–12

LEAKE, B.E., WOOLLEY, A.R., ARPS, C.E.S., BIRCH, W.D., GILBERT, M.C., GRICE, J.D., HAWTHOPNE, F.C., KATO, A., KISCH, H.J., KRIVOVICHEV, V.G., LINTHOUT, K., LAIRD, J., MANDARINO, J., MARESCH, W.V., NICKEL, E.H., ROCK, N.M.S., SCHUMACHER, J.C., SMITH, D.C., STEPHENSON, N.C.N., UNGARETTI, L., WHITTAKER, E.J.W., YOUZHI, G. 1997. Nomenclature of amphiboles: report of subcommittee on amphiboles of the international mineralogical association commission on new minerals and mineral names. *European Journal of Mineralogy* 9, 623–651.

MARUYAMA, S., SUZUKI, K. & LIOU, J.G. 1983. Greenschist-amphibolite transition equilibria at low pressures. *Journal of Petrology* 24, 583–604.

MOODY, J.B., MEYER, D. & JENKINS, J.E. 1983. Experimental characterization of the greenschist / amphibolite boundary in mafic systems. *American Journal of Science* 283, 48–92.

OKAY, A.İ. 1996. Granulite facies gneisses from the Pulur region, eastern Pontides. *Turkish Journal of Earth Sciences* 5, 55–61.

OKAY, A.İ. & LEVEN, E.-JA. 1996. Stratigraphy and paleontology of the upper Paleozoic sequences in the Pulur (Bayburt) region, eastern Pontides. *Turkish Journal of Earth Sciences* 5, 145–155.

Okay, A.İ. & Şahintürk, Ö. 1997. Geology of the eastern Pontides. *In*: Robinson, A.G. (ed), *Regional and Petroleum Geology of the Black Sea and Surrounding Region*. American Association of Petroleum Geologists Memoir **68**, 291–311.

Okay, A.İ., Şahintürk, Ö. & Yakar, H. 1997. Stratigraphy and tectonics of the Pulur (Bayburt) region in the eastern Pontides. *Bulletin of the Mineral Research and Exploration Institute (MTA), Turkey* **119**, 1–24.

Pattison, D.R.M. 1989. P-T conditions and the influence of graphite on pelitic phase relations in the Ballachulish aureole, Scotland. *Journal of Petrology* **30**, 1219–1244.

Pattison, D.R.M. 1992. Stability of andalusite and sillimanite and the Al_2SiO_5 triple point: constraints from the Ballachulish aureole, Scotland. *Journal of Geology* **100**, 423–446.

Pattison, D.R.M. & Harte, B. 1997. The geology and evolution the Ballachulish igneous complex and aureole. *Scottish Journal of Geology* **33**, 1–29.

Pouchou, J.L. & Pichoir, F. 1984. A new model for quantitative analyses. I. Application to the analysis of homogeneous samples. *La Recherche Aérospatiale* **3**, 13–38.

Pouchou, J.L. & Pichoir, F. 1985. "PAP" (Φ-ρ-Z) correction procedure for improved quantitative microanalysis. *In*: Armstrong, J.T. (ed), *Microbeam Analysis*, 104–106, San Francisco Press.

Rosing, M.T., Bird, D.K. & Dymek, R.F. 1987. Hydration of corundum-bearing xenoliths in the Qorqut granite complex, Godthabsfjord, west Greenland. *American Mineralogist* **72**, 29–38.

Sadiklar, M.B. 1993. Granat-Pyroxen-Rhytmite bei Özdil/Trabzon, NE-Türkei. *Chemie der Erde* **53**, 341–353.

Sakakibara, M. & Isono, Y. 1996. Middle Miocene thermal metamorphism due to the infiltration of high-temperature fluid in the Sanbagawa metamorphic belt, southwest Japan. *Contribution to Mineralogy and Petrology* **125**, 341–358.

Schumacher, J.C. 1997. The estimation of ferric iron in electron microprobe analyses of amphiboles. *European Journal of Mineralogy* **9**, 643–651.

Spear, F.S. 1981. An experimental study of hornblende stability in amphibolite. *American Journal of Science* **281**, 697–734.

Spear, F.S. 1993. *Metamorphic Phase Equilibria and Pressure-Temperature-Time Paths.* Mineralogical Society of America, Monograph.

Taner, M.F. 1977. *Étude géologique et pétrographique de la région de Güneyce-Ikizdere, située au sud de Rize (Pontides orientales, Turquie).* PhD Thesis, University of Geneve, 180 p [unpublished, in French].

Topuz, G. & Altherr, R. 2004. Pervasive rehydration of granulites during exhumation - an example from the Pulur complex, eastern Pontides, Turkey. *Mineralogy and Petrology* **81**, 165–185.

Topuz, G., Altherr, R., Satir, M. & Schwarz, W.H. 2004a. Low grade metamorphic rocks from the Pulur complex, NE Turkey: implications for pre-Liassic evolution of the eastern Pontides. *International Journal of Earth Sciences* **93**, 72–91.

Topuz, G., Altherr, R., Kalt, A., Satir, M., Werner, O. & Schwarz, W.H. 2004b. Aluminous granulites from the Pulur complex, NE Turkey: a case of partial melting, efficient melt extraction and crystallization. *Lithos* **72**, 183–207.

Topuz, G., Altherr, R., Schwarz, W.H., Siebel, W., Satir, M. & Dokuz, A. 2005. Post-collisional plutonism with 'adakite-like' signatures: the Eocene Saraycık granodiorite (Eastern Pontides, Turkey). *Contributions to Mineralogy and Petrology* **150**, 441–455.

Wheeler, J., Mangan S.L. & Prior, D.J. 2004. Disequilibrium in the Ross of Mull Contact metamorphic aureole, Scotland: a consequence of polymetamorphism. *Journal of Petrology* **45**, 835–853.

Yilmaz-Şahin, S. 2005. Transition from arc- to post-collision extensional setting revealed by K-Ar dating and petrology: an example from the granitoids of the Eastern Pontide Igneous Terrane, Araklı-Trabzon, NE Turkey. *Geological Journal* **40**, 425–440.